



Electrostatic Solitary Waves in the Venusian Ionosphere Pervaded by the Solar Wind: A Theoretical Perspective

R. Rubia¹, S. V. Singh², G. S. Lakhina², S. Devanandhan², M. B. Dhanya¹, and T. Kamalam³¹Space Physics Laboratory, Vikram Sarabhai Space Center, Thiruvananthapuram, Kerala, 695021, India; rubi.r92@gmail.com²Indian Institute of Geomagnetism, Navi Mumbai, 410218, India³School of Physics and Astronomy, University of Southampton, Southampton, SO17 1BJ, UK

Received 2022 December 27; revised 2023 April 26; accepted 2023 April 27; published 2023 June 15

Abstract

Electrostatic solitary waves (ESWs) in the Venusian ionosphere that are impinged by the solar wind are investigated using a homogeneous, collisionless, and magnetized multicomponent plasma consisting of Venusian H^+ and O^+ ions, Maxwellian Venusian electrons and streaming solar wind protons, and suprathermal electrons following κ – distribution. The model supports the propagation of positive potential slow O^+ and H^+ ion-acoustic solitons. The evolution and properties of the solitons occurring in two sectors, viz., dawn-dusk and noon-midnight sector of the Venus ionosphere at an altitude of (200–2000) km, are studied. The theoretical model predicts positive potential solitons with amplitude $\sim(0.067\text{--}56)$ mV, width $\sim(1.7\text{--}53.21)$ m, and velocity $\sim(1.48\text{--}8.33)$ km s^{-1} . The bipolar soliton electric field has amplitude $\sim(0.03\text{--}27.67)$ mV m^{-1} with time duration $\sim(0.34\text{--}22)$ ms. These bipolar electric field pulses when Fourier transformed to the frequency domain occur as a broadband electrostatic noise, with frequency varying in the range of ~ 9.78 Hz–8.77 kHz. Our results can explain the observed electrostatic waves in the frequency range of 100 Hz–5.4 kHz in the Venus ionosphere by the Pioneer Venus Orbiter mission. The model can also be relevant in explaining the recent observation of ESWs in the Venus magnetosheath by the Solar Orbiter during its first gravity assist maneuver of Venus.

Unified Astronomy Thesaurus concepts: [Venus \(1763\)](#); [Solar wind \(1534\)](#)

1. Introduction

Venus is often referred as “Earth’s twin” by virtue of its similarities in terms of size and structure. However, the interaction of the solar wind with the Venus is markedly different from that of the Earth with its internal magnetic field. The solar extreme ultraviolet radiation (EUV) and energetic particles partially ionize the thick neutral atmosphere/exosphere of Venus (producing photoions and photoelectrons), thereby generating the Venusian ionosphere (Zhang et al. 2007). Owing to the weak intrinsic magnetic field of Venus (Phillips & Russell 1987), the solar wind directly interacts with the ionosphere (Luhmann 1986). The solar wind magnetic field induces current in the conducting ionosphere, which in turn generates an induced magnetic field that inhibits the inflow of solar wind and interplanetary magnetic field (IMF) (Futaana et al. 2017). This spawns an “induced magnetosphere” (see Figure 1) that is analogous to Earth’s magnetosphere with regard to plasma regions but differs in spatial scale (Zhang et al. 2007; Futaana et al. 2017). When the solar wind traversing at supersonic speed encounters the induced magnetosphere, it is slowed down and deflected by the induced magnetosphere, which ensues in an upstream bow shock and downstream magnetotail. The Venusian magnetosphere is bounded by ionopause/magnetopause, where the solar wind dynamic pressure is approximately balanced by the thermal pressure of Venus’s ionospheric plasma. The ionopause on the night side acts as a boundary between the magnetosheath and the magnetotail. The magnetosheath region between the shock and the ionopause comprises thermalized subsonic solar wind

plasma, which is associated with piled-up and draped IMF (Futaana et al. 2017). The dynamics of Venus’s induced magnetosphere rely to a large extent on the solar activity (Zhang et al. 2007; Yadav 2020).

The interaction between the solar wind and Venus’s induced magnetosphere facilitates the existence of numerous linear and nonlinear plasma waves and turbulences (Futaana et al. 2017). Plasma waves play a prominent role in the energy transportation, particle heating and acceleration of particles to high energies, and modifying the particle distribution function. Furthermore, the waves can be utilized as a diagnostic tool to explore Venus’s ionosphere and its extended exospheres (Strangeway 1991; Futaana et al. 2017). Despite several spacecraft missions (including flybys, orbiters, and landers) to Venus, the quantum of information on the waves observed in the Venus is provided by the Orbiter Electric Field Detector (OEFD) on board the PVO (Russell et al. 2006). Scarf et al. (1979) reported the first ever observation of plasma waves in the Venus atmosphere, on the basis of PVO traversing the dawn-dusk (DD) sector during low solar activity. They observed the largest amplitude waves (inferred as whistler waves with frequency ~ 100 Hz) at very low altitudes (< 380 km), which are closer to the ionospheric boundary. They also reported the observation of ion-acoustic waves (with frequencies ~ 730 Hz and 5.4 kHz) and electron plasma waves (~ 30 kHz) generated by suprathermal electrons. Strangeway (1991) suggested the existence of electrostatic ion-acoustic or lower hybrid waves at the ionopause based on the results of Elphic et al. (1980). The broadband wave noise that is observed in the plasma cloud above the Venus ionosphere was elucidated in terms of ion-acoustic waves by Scarf et al. (1985). The plasma cloud is a detached volume of ionospheric plasma that is observed above the ionosphere and is often associated with wave activities having similar characteristics to those appearing in the ionopause (Brace et al. 1982; Russell et al. 1982). The occurrence of ion-



Original content from this work may be used under the terms of the [Creative Commons Attribution 4.0 licence](#). Any further distribution of this work must maintain attribution to the author(s) and the title of the work, journal citation and DOI.

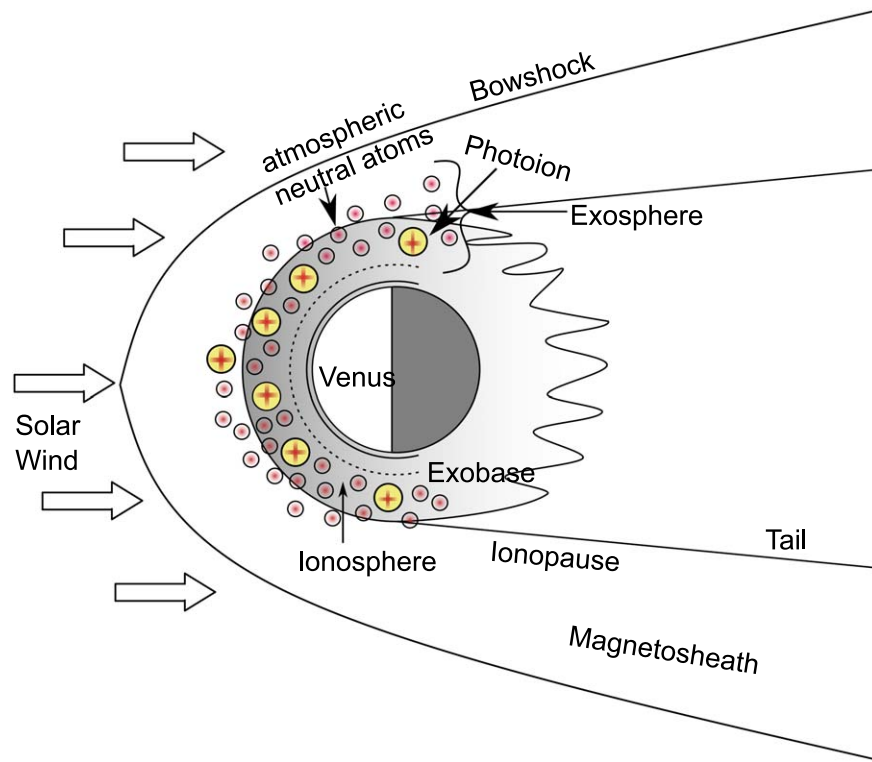


Figure 1. A schematic of the Venusian induced magnetosphere (not to scale).

acoustic waves in the magnetotail region was investigated by Intriligator & Scarf (1984).

ESWs are ubiquitous in space plasma environment, viz., planetary magnetospheres (Matsumoto et al. 1994; Kurth et al. 2001; Pickett et al. 2005; Williams et al. 2006), solar wind (Mangeny et al. 1999), lunar wake (Hashimoto et al. 2010), and so on. Generally, the ESWs are accountable for the generation of broadband electrostatic noise (BEN) or electrostatic turbulence in the space plasma environment (Matsumoto et al. 1994; Lakhina et al. 2000). In the literature, a large number of theoretical studies on the generation mechanism, structure, and properties of the ESWs in various space plasma environments are available (Lakhina et al. 2021a, Reddy & Lakhina 1991; Lakhina & Singh 2015; Rubia et al. 2016, 2017; Lakhina et al. 2018, 2021a) (For further details, kindly refer Lakhina et al. 2018, 2021b and references therein.) However, research on the nature of ESWs in the Venus ionosphere pervaded by the solar wind is limited. Recent spacecraft missions that flyby Venus for gravity assist maneuver have reported the occurrence of ESWs and double layers in the induced Venus magnetosphere. Hadid et al. (2021) reported the occurrence of ESWs with peak-to-peak electric field amplitude of a few mV m^{-1} with a characteristic timescale of ~ 0.5 ms in the magnetosheath and the tail region of the Venus on the basis of Time Domain Sampler (TDS) on board the Solar Orbiter. They interpreted these structures as electron phase space holes propagating parallel to the ambient magnetic field. Malaspina et al. (2020) reported the Parker Solar Probe (PSP) observation of electron phase space holes and double layers (with spatial scales of few tens of Debye lengths and potential drops of few tens of V) near the bow shock. Moslem et al. (2018) investigated shocklike solitons and small amplitude double layers in the interaction region of the solar wind with the Venus ionosphere. Salem et al. (2019) studied the mechanism for the

ionic losses from the Venus ionosphere by virtue of interaction between the solar wind and the Venus ionosphere. They employed a hydrodynamic approach in a multicomponent plasma to inspect the correlation between plasma density, velocity, electric potential, and solar wind parameters. They predicted that O^+ ions to electrons relative density are a key factor for ionic loss in the noon-midnight (NM) sector. Meanwhile, in the DD sector, all the ion densities (O^+ , H^+ and solar wind protons) play an important role in either increasing or decreasing the ionic losses. However, streaming solar wind velocity does not contribute toward the escape of Venusian ions in either the DD or NM sectors at low altitudes. Prasad et al. (2021) reported the occurrence of ion-acoustic solitary, periodic, and superperiodic waves in the NM sector as a result of ionospheric escape from the Venus atmosphere by utilizing the Sagdeev pseudopotential analysis on the plasma model of Salem et al. (2019). Sayed et al. (2020) investigated the propagation of nonlinear ion-acoustic waves in Venus's plasma environment. They modeled the Venus plasma using a three-component plasma consisting of H^+ and O^+ ions and electrons following Maxwellian distribution. They reported that only compressive ion-acoustic solitons propagating with a speed of ~ 2 km s^{-1} exists in the Venus ionosphere at the altitude 200–1000 km. Afify et al. (2021) analyzed the linear and small amplitude nonlinear wave dynamics during the solar wind interaction with the upper atmosphere of the Venus. Using the reductive perturbation method, they predicted the electric field amplitude of the ESWs as 1.2 mV m^{-1} with time duration of 0.4 ms and proposed that these ESWs could provide a plausible explanation for the plasma oscillations detected during the Galileo flyby of Venus (Gurnett et al. 1991).

The preceding theoretical studies used either Maxwellian or fluid description for the electrons. However, in space plasma, the distribution function is often observed to deviate from the

Maxwellian distribution due to the presence of suprathermal electrons having high energy tails (Vasyliunas 1968; Leubner 1982). Generally, such suprathermal particles are effectively described using κ -distribution (Summers & Thorne 1991). In this paper, we study the characteristics of ESWs in Venus's ionosphere pervaded by the solar wind, using a multicomponent plasma comprising of Venusian H^+ and O^+ ions, background Venusian electrons following Maxwellian distribution, and streaming solar wind protons and suprathermal electrons following drift- κ distribution, in terms of ion-acoustic solitons. The solar wind electron population has three components, viz. cold "core," hot "halo," and strahl. The slow solar wind is often characterized by "core" and "halo" electrons, while the fast solar wind consists of all three components (Pierrard & Lemaire 1996). Generally, the number density of the strahl component is lesser than the core electrons, and hence has been neglected in our study. The core and halo electrons taken together can effectively be modeled using κ -distribution (Lakhina & Singh 2015). On the basis of numerous kinetic models and satellite observations of the electron distribution function, it has been established that κ distribution can effectively model the solar wind electrons for both slow (large values of κ) and fast (lower κ values) solar wind conditions better than the Maxwellian distribution (Pierrard & Lemaire 1996; Maksimovic et al. 1997a, 1997b). We would like to emphasize that the κ -distribution considered here describes the total electron distribution and not just the suprathermal part because one would obtain the Maxwellian distribution for large values of κ (core part) and suprathermal part for low values of κ , which justifies the modeling of the solar wind electrons using κ -distribution.

The generation of ESWs is governed by two main mechanisms, viz., BGK (Bernstein–Green–Kruskal) modes, phase space holes, and ion- or electron-acoustic solitons and double layers. The trapped particle population is vital in the BGK generation mechanism. Numerous kinetic simulations have demonstrated that the nonlinear saturation of electron beam instabilities generates isolated potential structures, analogous to the BGK modes/phase space holes that emulate ESWs. However, the phase space holes were found to be unstable with a tendency to merge or breakup as the instability evolves. The soliton and double layer generation mechanism utilizes the fluid model to describe the evolution of ESWs (for further details on the merits of the soliton model, kindly refer Lakhina et al. 2018, 2021b). Here, we emphasise that our model considers only the time-stationary state of the plasma system. In such a state, plasma instabilities, if present initially, would have been saturated. The model deals only with the nonlinear states of the system. Here, Section 2 provides the theoretical plasma model that we used and Section 3 discusses the numerical results. Section 4 compares the results of the theoretical model with previous theoretical studies of ESWs occurring in the Venus ionosphere. The conclusions are given in Section 5.

2. Theoretical Model

The PVO and Venus Express (VEX) observations of the Venus ionosphere indicate O^+ and H^+ ions (ionospheric and solar wind origin) and electrons as the dominant species in the ionosphere above an altitude of 200 km (above exobase) (Knudsen 1992; Lundin et al. 2011). These observations motivated us to model the interaction region of the solar wind

plasma with Venus's ionosphere using a homogeneous, collisionless, and magnetized multicomponent plasma comprising of positive ions ($H^+(N_{vh0}, T_{vh})$ and $O^+(N_{vo0}, T_{vo})$) of Venusian origin, background Venusian electrons (N_{be0}, T_{be}) following Maxwellian distribution and streaming solar wind protons (N_{sp0}, T_{sp}, V_0) and suprathermal electrons following κ -distribution (N_{se0}, T_{se}, V_0), where N_{j0} , T_j and V_0 represents the equilibrium values of the number density, temperature, and streaming velocity (in the direction of the ambient magnetic field, \mathbf{B}_0), respectively, for the j^{th} species, with $j = \text{vh}, \text{vo}, \text{be}, \text{sp}$, and se , respectively, corresponding to Venusian H^+ ions and O^+ ions, Venusian electrons, solar wind protons, and electrons. Here, both the solar wind protons and electrons are considered to be streaming with same velocity, V_0 .

The solar wind electrons streaming with velocity V_0 are considered to follow the drifting κ -distribution given by Liu & Du (2009)

$$f_{se}(V) = \frac{N_{se0}}{\sqrt{\pi}\theta} \frac{\Gamma(\kappa + 1)}{\kappa^{3/2} \Gamma(\kappa - 1/2)} \left(1 + \frac{(V - V_0)^2}{\kappa\theta^2} \right)^{-\kappa} \quad (1)$$

where, κ is the spectral index with $\kappa > 3/2$, $\Gamma(\kappa)$ is the gamma function and $\theta^2 = \left(2 - \frac{3}{\kappa} \right) \frac{T_{se}}{m_e}$, is the modified solar wind electron thermal speed. T_{se} and m_e represents the solar wind electron temperature and mass, respectively. When $\kappa \rightarrow \infty$, the drift κ -distribution approaches drift Maxwellian distribution.

The solar wind electron number density in the presence of electrostatic wave having electric potential ϕ can be attained by substituting $\frac{(V - V_0)^2}{\theta^2}$ by $\frac{(V - V_0)^2}{\theta^2} - \frac{2e\phi}{m_e\theta^2}$ in Equation (1) and integrating it over the velocity space (Rubia et al. 2017; Singh et al. 2020),

$$n_{se} = n_{se0} \left(1 - \frac{\phi}{\kappa - 3/2} \right)^{-\kappa+1/2}. \quad (2)$$

As the background electrons follow Maxwellian distribution, their number density in the presence of electrostatic waves with potential, ϕ is given as (Lakhina et al. 2014, 2020)

$$n_{be} = n_{be0} \exp\left(\frac{\phi}{\sigma_{be}}\right). \quad (3)$$

Here, ϕ is normalized with T_{se}/e and $\sigma_{be} = T_{be}/T_{se}$.

The underlying fluid equations govern the dynamics of the Venusian H^+ and O^+ ions and solar wind protons in the interaction region of the solar wind with the Venus ionosphere,

$$\frac{\partial n_j}{\partial t} + \frac{\partial(n_j v_j)}{\partial x} = 0 \quad (4)$$

$$\frac{\partial v_j}{\partial t} + v_j \frac{\partial v_j}{\partial x} + \mu_{spj} \frac{\partial \phi}{\partial x} + 3\mu_{spj} \sigma_j \frac{n_j}{n_{j0}} \frac{\partial n_j}{\partial x} = 0 \quad (5)$$

$$\frac{\partial^2 \phi}{\partial \xi^2} = (n_{se} + n_{be} - n_{vh} - n_{vo} - n_{sp}). \quad (6)$$

Equations (2)–(6) are normalized equations. Number densities are normalized with the equilibrium number density of electrons (or ions), $N_0 = N_{vh0} + N_{vo0} + N_{sp0} = N_{se0} + N_{be0}$. Velocities are normalized with ion-acoustic speed, $C_a = \sqrt{T_{se}/m_{sp}}$; m_{sp} is the mass of the proton and T_{se} is the temperature of the solar wind electron, lengths are normalized using effective hot electron Debye length, $\lambda_{dse} = \sqrt{T_{se}/4\pi N_0 e^2}$, time is normalized using inverse of the proton

plasma frequency, $\omega_{pp} = \sqrt{4\pi N_0 e^2 / m_{sp}}$, and electrostatic potential, ϕ is normalized with T_{se}/e . Here, $j = \text{vh}, \text{vo}, \text{sp}$ denote Venusian H^+ and O^+ ions and solar wind protons, respectively. $\sigma_j = T_j/T_{se}$ and $n_{j0} = N_j/N_0$ represents the normalized temperature and equilibrium number density,

$$\begin{aligned}
S(\phi, M) = & \frac{n_{\text{vh}0}}{6\sqrt{3}\sigma_{\text{vh}}} \left\{ \left[\left(\frac{M}{\sqrt{\mu_{\text{spvh}}}} + \sqrt{3\sigma_{\text{vh}}} \right)^3 - \left[\left(\frac{M}{\sqrt{\mu_{\text{spvh}}}} + \sqrt{3\sigma_{\text{vh}}} \right)^2 - 2\phi \right]^{3/2} \right. \right. \\
& \left. \left. - \left(\frac{M}{\sqrt{\mu_{\text{spvh}}}} - \sqrt{3\sigma_{\text{vh}}} \right)^3 + \left[\left(\frac{M}{\sqrt{\mu_{\text{spvh}}}} - \sqrt{3\sigma_{\text{vh}}} \right)^2 - 2\phi \right]^{3/2} \right\} \\
& + \frac{n_{\text{vo}0}}{6\sqrt{3}\sigma_{\text{vo}}} \left\{ \left[\left(\frac{M}{\sqrt{\mu_{\text{spvo}}}} + \sqrt{3\sigma_{\text{vo}}} \right)^3 - \left[\left(\frac{M}{\sqrt{\mu_{\text{spvo}}}} + \sqrt{3\sigma_{\text{vo}}} \right)^2 - 2\phi \right]^{3/2} \right. \right. \\
& \left. \left. - \left(\frac{M}{\sqrt{\mu_{\text{spvo}}}} - \sqrt{3\sigma_{\text{vo}}} \right)^3 + \left[\left(\frac{M}{\sqrt{\mu_{\text{spvo}}}} - \sqrt{3\sigma_{\text{vo}}} \right)^2 - 2\phi \right]^{3/2} \right\} \\
& + \frac{n_{\text{sp}0}}{6\sqrt{3}\sigma_{\text{sp}}} \{ ((M - v_0) + \sqrt{3\sigma_{\text{sp}}})^3 - [((M - v_0) + \sqrt{3\sigma_{\text{sp}}})^2 - 2\phi]^{3/2} \\
& - ((M - v_0) - \sqrt{3\sigma_{\text{sp}}})^3 + [((M - v_0) - \sqrt{3\sigma_{\text{sp}}})^2 - 2\phi]^{3/2} \} \\
& + n_{\text{se}0} \left\{ 1 - \left(1 - \frac{\phi}{\kappa - 3/2} \right)^{-\kappa+3/2} \right\} + n_{\text{be}0} \sigma_{\text{be}} \left\{ 1 - \exp\left(\frac{\phi}{\sigma_{\text{be}}} \right) \right\}. \tag{8}
\end{aligned}$$

respectively. Here, $\mu_{\text{spj}} = m_{\text{sp}}/m_j$, where m_j is the mass of the j^{th} species. Ion-acoustic wave exists when the condition, $v_{\text{thi}} \ll v_{\text{ph}} \ll v_{\text{the}}$ holds. Here, v_{thi} and v_{the} is the thermal velocity of the ions and electrons, respectively; v_{ph} is the phase velocity of the wave (Salem et al. 2022). The electrons move much more quickly in comparison to the waves and have sufficient time to maintain equal temperature everywhere. Hence, the electrons are isothermal. In comparison to electron timescale, the ions being massive move relatively slowly with respect to the waves, resulting in adiabatic compression. Hence, we have considered the adiabatic index, $\gamma_j = 3$.

To analyze the properties of the ESWs, we transform Equations (4)–(6) to a stationary frame moving with phase velocity, V of the ESWs, i.e., $\xi = x - Mt$, where $M = V/C_a$ depicts the Mach number. We obtain the number densities of Venusian H^+ and O^+ ions and solar wind protons by solving Equations (4)–(5), along with appropriate boundary conditions (i.e., all variables, viz., fluid velocities, densities approaches their equilibrium values, and the electrostatic potential, $\phi = 0$ and $d\phi/d\xi = 0$ at $\xi \rightarrow \infty$). The resulting number density, along with the number density of solar wind electrons (Equation (2)) and background electrons (Equation (3)), is substituted in the Poisson's Equation (6) and solved using the appropriate boundary condition to obtain the energy integral, as in Lakhina & Singh (2015) and Lakhina et al. (2021b)

$$\frac{1}{2} \left(\frac{d\phi}{d\xi} \right)^2 + S(\phi, M) = 0. \tag{7}$$

Equation (7) represents the motion of a pseudoparticle of unit mass in a pseudopotential, $S(\phi, M)$, with ϕ and ξ , respectively depicting pseudo-displacement from the equilibrium and pseudo-time (Lakhina et al. 2009; Rubia et al. 2017; Lakhina et al. 2020). The Sagdeev pseudopotential, $S(\phi, M)$, is given by

Equation (8) is represented in an allegorical form where the operation of a square root on a squared expression results in the same expression, e.g., $\sqrt{(M \pm \sigma_j)^2} = M \pm \sigma_j$. Here, $v_0 = V_0/C_a$ is the normalized drift speed of the solar wind electrons and protons.

The Sagdeev pseudopotential, $S(\phi, M)$ must comply with the following conditions for the existence of soliton solution (Lakhina et al. 2018; Rubia et al. 2018; Lakhina et al. 2021a): (i) $S(\phi, M) = 0$, $dS(\phi, M)/d\phi = 0$, and $d^2S(\phi, M)/d\phi^2 < 0$ at $\phi = 0$, (ii) $S(\phi, M) = 0$ at $\phi = \phi_{\text{max}}$ (ϕ_{max} is the maximum attainable amplitude of the soliton), and (iii) $S(\phi, M) < 0$ for $0 < |\phi| < |\phi_{\text{max}}|$.

From Equation (8), it can be observed that the Sagdeev pseudopotential, $S(\phi, M)$ and its first derivative with respect to ϕ ($dS(\phi, M)/d\phi$) becomes null at $\phi = 0$. Moreover, the soliton condition $d^2S(\phi, M)/d\phi^2 < 0$ at $\phi = 0$ requires that $M > M_0$, where the critical Mach number, M_0 , above which the soliton solution exists, satisfies the underlying equation:

$$\begin{aligned}
& \frac{n_{\text{vh}0}}{\frac{M^2}{\mu_{\text{spvh}}} - 3\sigma_{\text{vh}}} + \frac{n_{\text{vo}0}}{\frac{M^2}{\mu_{\text{spvo}}} - 3\sigma_{\text{vo}}} \\
& + \frac{n_{\text{sp}0}}{(M - v_0)^2 - 3\sigma_{\text{sp}}} = n_{\text{se}0} \left(\frac{\kappa - 1/2}{\kappa - 3/2} \right) + \frac{n_{\text{be}}}{\sigma_{\text{be}}}. \tag{9}
\end{aligned}$$

For admissible parameters corresponding to the interaction region of the solar wind with Venus's ionosphere, Equation (9) is numerically solved to obtain the M_0 . Equation (9) supports

Table 1

Number Density of the Venusian H^+ and O^+ Ions and Solar Wind Protons for the DD and NM Sectors at Different Altitudes of Venus's Ionosphere

Altitude	DD			NM		
	N_{vh0} (cm^{-3})	N_{vo0} (cm^{-3})	N_{sp0} (cm^{-3})	N_{vh0} (cm^{-3})	N_{vo0} (cm^{-3})	N_{sp0} (cm^{-3})
2000 km	15	0.6	40	3.5	3	4.5
1000 km	40	50	10	15	45	15
800 km	40	50	8.5	11	60	10
600 km	28	100	6	10	100	8.5
400 km	15	180	5	7.5	190	3.5
200 km	1	200	5	5	200	1

six roots, of which all are not physical. Here, we analyze only the real positive roots. The roots with same magnitude but negative sign exhibit similar properties as those of the positive roots (propagating parallel to B_0) but propagates in the opposite direction (i.e., antiparallel to B_0). The relative ordering of the species thermal velocities and the physical roots (unnormalized velocities) determines the nature of the root obtained (Lakhina et al. 2008). For the parameters that we considered, we observe that the lowest velocity (root) is greater than the thermal velocity of O^+ ions but is lesser than that of H^+ ions. The intermediate velocity (root) lies between the thermal velocities of H^+ ions and solar wind protons. Meanwhile, the largest velocity (root) lies between the thermal velocities of solar wind protons and electrons: $V_{tvo} < V_{lowest} < V_{tvh} < V_{intermediate} < V_{tsp} < V_{largest} < V_{tbe} < V_{tse}$. The lowest and the intermediate root corresponds to slow O^+ and H^+ ion-acoustic mode, respectively, while the largest root corresponds to the fast ion-acoustic mode (Lakhina et al. 2014; Lakhina & Singh 2015; Rubia et al. 2016). The fast ion-acoustic mode is similar to the regular ion-acoustic mode occurring in a proton-electron plasma. Meanwhile, the slow ion-acoustic mode is an ion-ion hybrid mode, essentially requiring two or more ion species either having different thermal velocities or relative streaming between the ions (Lakhina & Singh 2015; Lakhina et al. 2018). For the parameters relevant to Venus's ionosphere, only slow O^+ and H^+ ion-acoustic modes support the propagation of solitons.

3. Numerical Results and Discussions

For pertinent parameters corresponding to the Venus ionosphere permeated by the solar wind, Equation (8) is numerically solved for $S(\phi, M)$ varying with ϕ for different values of Mach number, $M \geq M_0$. Subsequently, Equation (7) and Equation (8) are simultaneously solved using the RK-4 method (Singh et al. 2020) to obtain the potential and electric field profiles. The numerical analysis of our theoretical model is carried out on the basis of the observations provided by Lundin et al. (2011). The altitude profiles (ion density, ion velocity, and ion-mass flux) for the DD and NM sector of the Venus ionosphere were analyzed by Lundin et al. (2011) based on the observations of the ASPERA-4 Ion Imaging Analyzer (IMA) on board the 390 Venus Express (VEX) satellite. In the NM meridian, H^+ and O^+ ions and electrons were the major constituents at an altitude of 200–10,000 km (Lundin et al. 2011; Prasad et al. 2021). Meanwhile, in the DD meridian, H^+ and O^+ ions and electrons are dominant species at an altitude below 2000 km. For higher altitudes, only H^+ and electrons are prevalent. We obtained the number densities of the Venusian

H^+ and O^+ ions and solar wind protons at different altitudes for both NM and DD sectors from Figures 8 and 9 of Lundin et al. 2011, respectively. Table 1 summarizes the number density of the Venusian H^+ and O^+ ions and solar wind protons considered at different altitudes of the Venus ionosphere for both DD and NM sectors. To satisfy the charge neutrality condition, we considered the number density of background electrons as $N_{be0} = N_{vh0} + N_{vo0}$ and the number density of solar wind electrons as $N_{se0} = N_{sp0}$. Temperature variation of the species with altitude is not available in the literature. Based on the observation at 0.7 au, we considered the temperature of Venusian H^+ and O^+ as 1000 K and that of the background Venusian electrons as $T_{be} = 5000$ K. The temperature of the solar wind protons and electrons is taken as $T_{sp} = 10^5$ K and $T_{se} = 2 \times 10^5$ K, respectively (Luhmann & Kozyra 1991; Russell et al. 2006).

Figure 2 (a) represents the variation of Sagdeev potential, $S(\phi, M)$ with ϕ for various Mach number values for slow O^+ ion-acoustic mode corresponding to the normalized parameters pertinent to the DD sector of the Venus ionosphere at an altitude of 1000 km: $n_{vh0} = 0.4$, $n_{vo0} = 0.5$, $n_{sp0} = 0.1$, $v_0 = 4.92$, $\sigma_{vh} = \sigma_{vo} = 0.005$, $\sigma_{sp} = 0.5$, $\sigma_{be} = 0.025$, and $\kappa = 2$. The amplitude of $S(\phi, M)$ increases with the increase in the Mach number until the maximum attainable Mach number, M_{max} is reached. Beyond M_{max} , the soliton solution does not exist. Here, M_{max} is provided by the requirement that the number density of the Venusian O^+ ions be real. Figure 2 (b) depicts the variation of potential ϕ with ξ . The solitons have symmetric profiles. The width of the solitons decreases, while the amplitude increases with increase in the Mach number. The bipolar electric field profiles of the solitons showing a similar trend to that of the potential profiles are represented in Figure 2(c). Figure 2 (d) represents the fast Fourier transform (FFT) power spectra of the unnormalized electric field (in $mV m^{-1}$). The frequency peak in the spectra occurs at 29.93 Hz, 40.16 Hz, 40.36 Hz, and 40.57 Hz corresponding to $M = 0.039$, 0.03925, 0.03945, and 0.03965, respectively. The maximum frequency contribution is in the range $\sim(9.78-927.73$ Hz), $\sim(10.14-431.71$ Hz), $\sim(10.14$ Hz–1.413 kHz), and $\sim(10.14$ Hz–1.92 kHz) for $M = 0.039$, 0.03925, 0.03945, and 0.03965, respectively. Here, the upper limit on the frequency, f , is taken at the cutoff power -50 dB. It is also observed that the power spectrum decreases with increase in frequency.

Figure 3 (a) shows the plots of $S(\phi, M)$ versus ϕ for slow H^+ ion-acoustic mode corresponding to the normalized parameters of Figure 2. The Sagdeev potential, normalized potential, and normalized electric field shows similar trend to that of respective profiles in Figure 2. Here, the limitation on the maximum amplitude of the soliton, M_{max} is provided by the requirement that the number density of the Venusian H^+ ions be real. Figure 3 (d) represents the FFT power spectra of the unnormalized electric field. The peak frequency in the spectra occurs at 130.83 Hz, 131.60 Hz, 132.60 Hz and 133.60 Hz for $M = 0.1705$, 0.1715, 0.1728 and 0.1741, respectively. The maximum contribution to the frequency lies in the range of $\sim(43.87$ Hz to 5.45 kHz), $\sim(44.2$ Hz to 6.76 kHz), $\sim(44.53$ Hz to 8.77 kHz), and $\sim(44.53$ Hz to 6.67 kHz) for $M = 0.1705$, 0.1715, 0.1728, and 0.1741, respectively. Here, the cutoff power is -50 dB.

Figure 4 shows the variation of the critical Mach number, M_0 , and maximum mach number, M_{max} , with n_{vh0} for both O^+ (panel-(a)) and H^+ ion-acoustic solitons (panel-(b)) for the normalized parameters corresponding to Figure 2. Both M_0 and

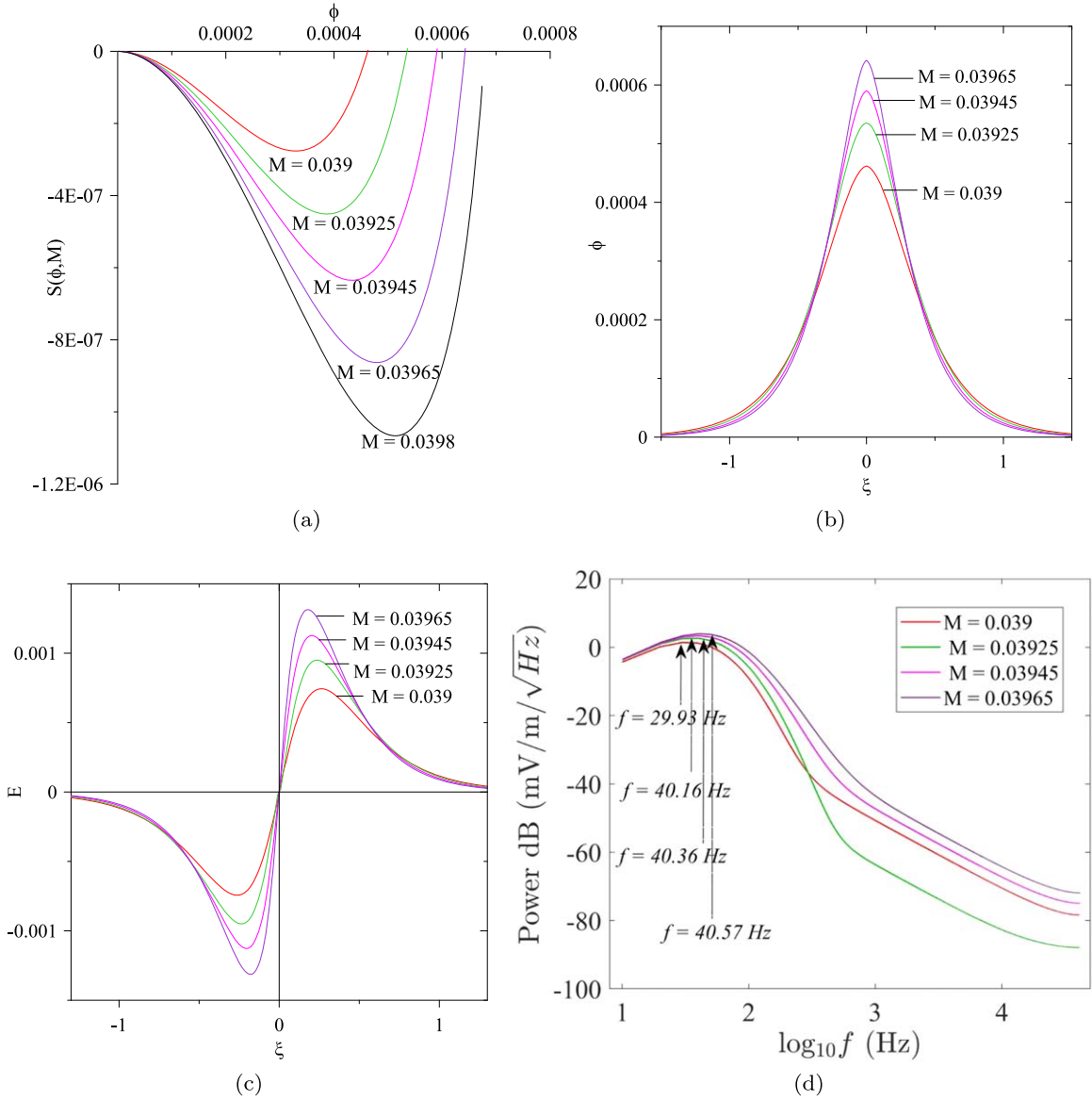


Figure 2. Panel (a) shows the plot of Sagdeev pseudopotential $S(\phi, M)$ vs. the potential ϕ for various Mach numbers depicted along the curves, corresponding to slow O^+ ion-acoustic mode for the normalized parameters applicable to the DD sector of Venus's ionosphere at an altitude of 1000 km: $n_{vh0} = 0.4$, $n_{v0} = 0.5$, $n_{sp0} = 0.1$, $v_0 = 4.92$, $\sigma_{vh} = \sigma_{v0} = 0.005$, $\sigma_{sp} = 0.5$, $\sigma_{be} = 0.025$, and $\kappa = 2$. Panel (b) shows the plot of normalized potential ϕ vs. ξ . Panel (c) shows the plot of the normalized electric field E varying with ξ . Panel (d) depicts the fast Fourier transform (FFT) power spectra of the unnormalized electric field (in $mV m^{-1}$) corresponding to different Mach numbers. The x-axis represents $\log_{10} f$, where f is the frequency in Hz. The y-axis represents the power of the electric field expressed in units of decibels, dB ($mV m^{-1} / \sqrt{Hz}$).

M_{max} decrease gradually with increasing n_{vh0} for O^+ ion-acoustic soliton. Meanwhile, both M_0 and M_{max} increase gradually with n_{vh0} . Since the Mach number for both O^+ and H^+ ion-acoustic modes with respect to solar wind proton ion-acoustic speed is less than 1, the solitons are considered as subsonic with respect to the solar wind proton ion-acoustic speed. Figure 5 depicts the variation of M_0 and M_{max} with σ_{sp} . For both O^+ and H^+ ion-acoustic solitons, M_0 and M_{max} remain nearly constant with an increase in σ_{sp} .

Figure 6 depicts the variation of the potential ϕ with ξ for different altitudes in both the DD and NM sectors corresponding to O^+ (panel-(a)) and H^+ (panel-(b)) ion-acoustic solitons. Solid and dashed lines represent the ion-acoustic solitons in DD and NM sector, respectively. The amplitude and width of O^+ ion-acoustic solitons increase with the decrease in

altitude for DD sector. Meanwhile, for the NM sector, the amplitude and width increase with a decrease in altitude up to 600 km, beyond which the amplitude decreases. In addition, the amplitude and width of the solitons is higher in NM than DD sector corresponding to a given altitude. For H^+ ion-acoustic mode, the amplitude and width decrease with altitude for both DD and NM sectors. In addition, the width and the amplitude of the solitons in the NM sector are less than those of the DD sector for a given altitude. These variations in the amplitude and width of the solitons in the DD and NM sectors for different altitudes are a consequence of the varying number densities with altitude.

Figure 7 illustrates the variation of potential profiles with varied values of (a) κ and (b) v_0 for H^+ ion-acoustic mode corresponding to DD sector at an altitude of 2000 km with

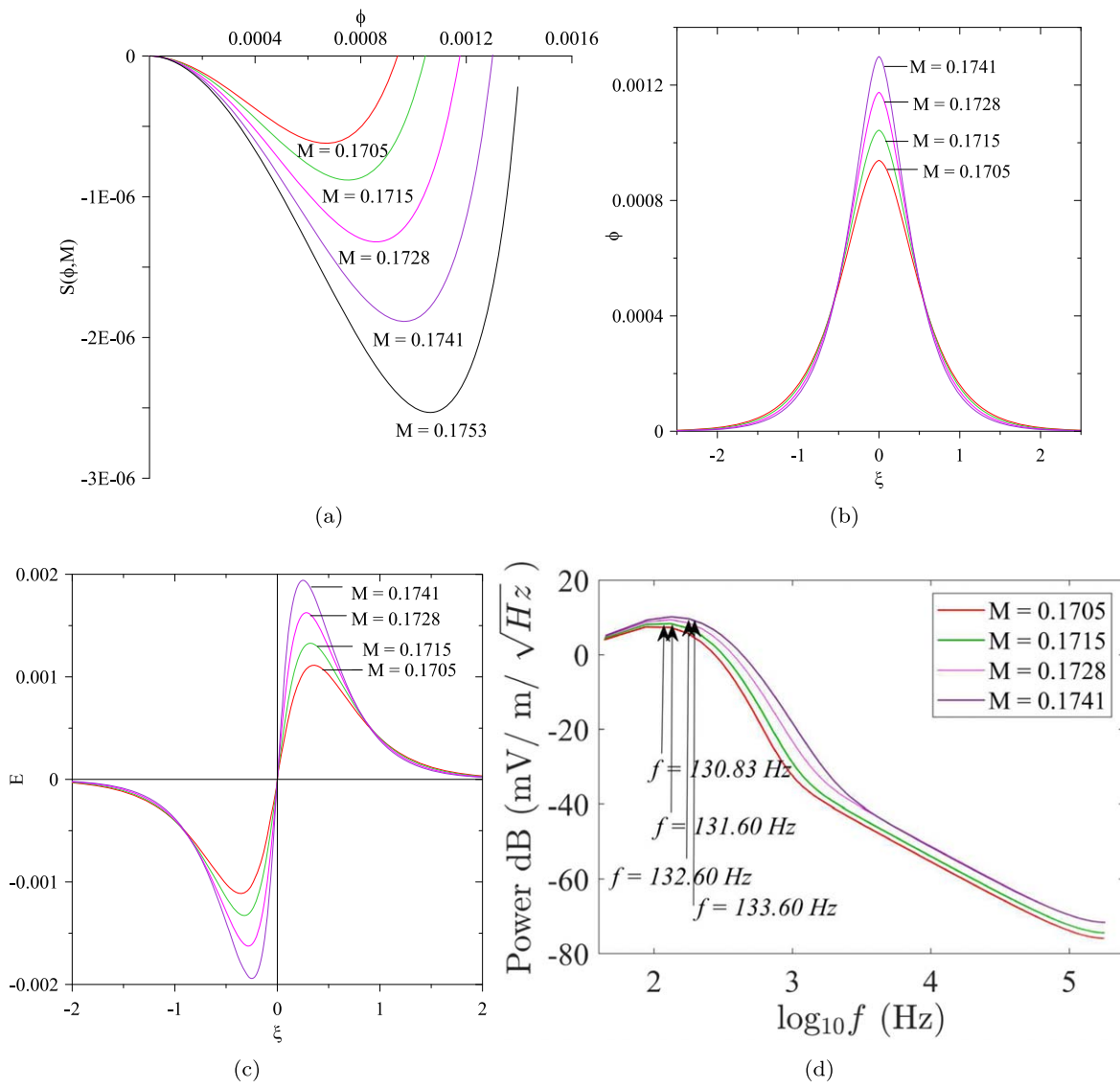


Figure 3. Panel (a) shows the variation of $S(\phi, M)$ with ϕ for slow H^+ ion-acoustic mode for normalized parameters corresponding to Figure 2. Panel (b) shows the plot of ϕ vs. ξ . Panel (c) shows the plot of E varying with ξ . Panel (d) depicts the FFT power spectra of the unnormalized electric field.

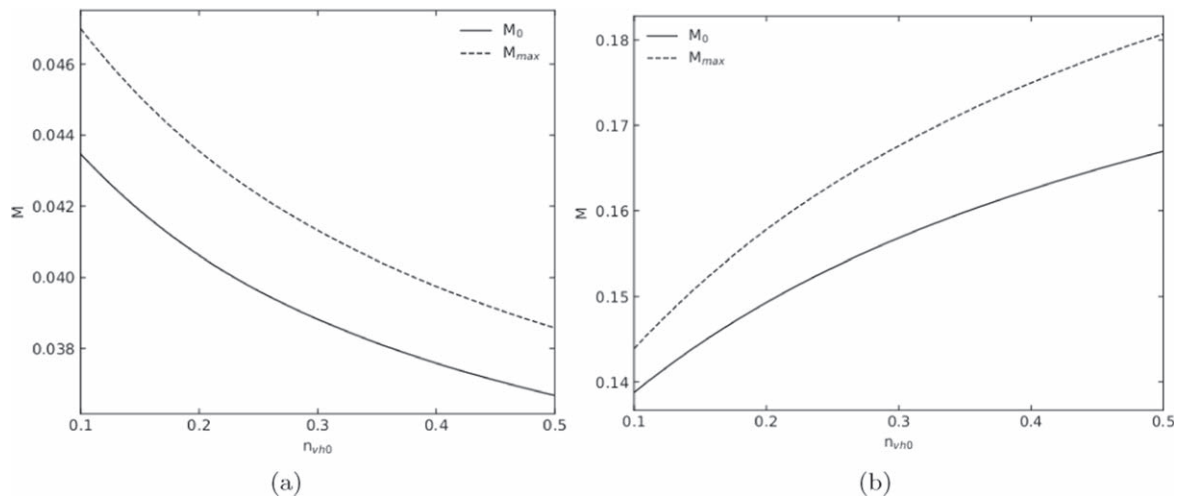


Figure 4. Variation of the critical Mach number (M_0) and maximum Mach number (M_{max}) with n_{vh0} for both (a) O^+ and (b) H^+ ion-acoustic mode for the normalized parameter corresponding to Figure 2.

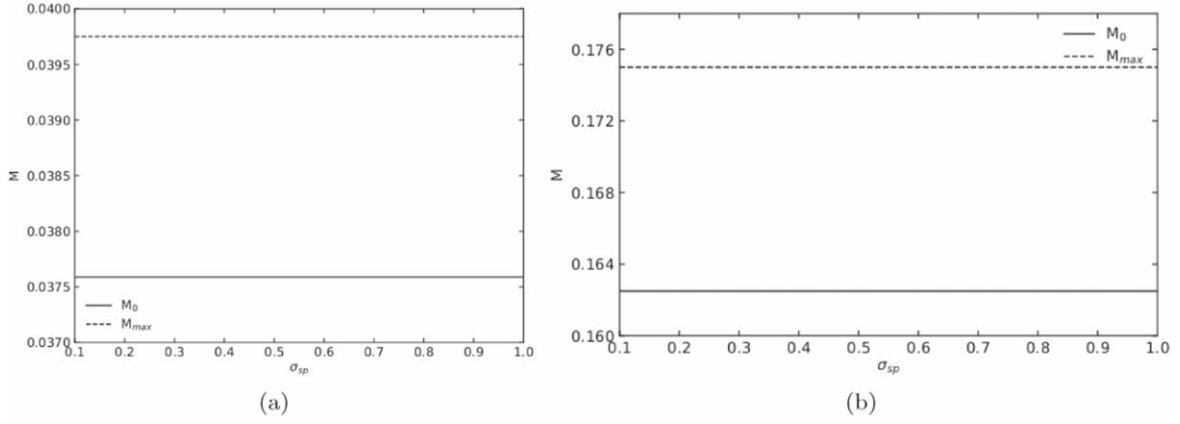


Figure 5. Variation of the critical Mach number (M_0) and maximum Mach number (M_{max}) with σ_{sp} for both (a) O^+ and (b) H^+ ion-acoustic mode for the normalized parameter corresponding to Figure 2.

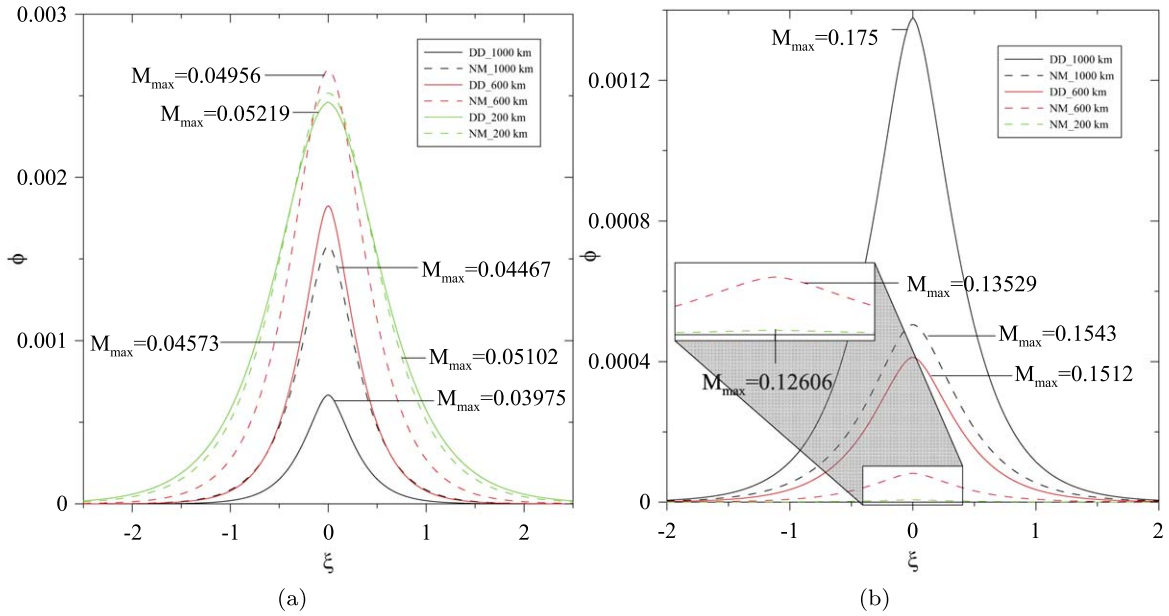


Figure 6. The variation of the potential ϕ with ξ is illustrated for different altitudes of the DD (solid lines) and NM (dashed lines) sectors. Panels (a) and (b) depicts O^+ and H^+ ion-acoustic modes, respectively. The normalized parameters considered are: $v_0 = 4.92$, $\sigma_{vh} = \sigma_{vo} = 0.005$, $\sigma_{sp} = 0.5$, $\sigma_{be} = 0.025$, and $\kappa = 2$ along with normalized number densities at different altitudes given in Table 1.

normalized parameters: $n_{vh0} = 0.27$, $n_{vo0} = 0.01$, $n_{sp0} = 0.72$, $\sigma_{vh} = \sigma_{vo} = 0.005$, $\sigma_{sp} = 0.5$, $\sigma_{be} = 0.025$, and $M = 0.2$. For the parameters considered, only H^+ ion-acoustic solitons exist because the number density of O^+ ions is less. From panel (a), we observe that with an increase in κ , the amplitude of the solitons decreases while the width increases. From panel (b), we see that the amplitude increases with v_0 . Furthermore, we observe that the effect of solar wind particles on the characteristics of the solitons is significant when the number density of the solar wind particles is above a threshold density ($n_{sp0} > 0.15$) and when the temperature of the solar wind electrons become comparable to that of the Venusian background electrons (which are not shown to conserve space).

In the DD sector corresponding to higher altitude ($10^3 - 10^4$) km, we also studied the variation in the soliton characteristics using the normalized parameters, viz., $n_{vh0} = 0.53$, $n_{vo0} = 0.31$, $n_{sp0} = 0.16$, $\sigma_{vh} = \sigma_{vo} = 0.25$, and $\sigma_{sp} = 1$, $\sigma_{be} = 1$, as given by Afify et al. (2021), who normalized the number density with the background Venusian electron number density. Hence, we converted the number density to our normalization,

i.e., equilibrium number density of ion/electrons. The potential ϕ varying with ξ for varied values of κ is illustrated in Figure 8. Panels (a) and (b) show the potential profile for O^+ and H^+ ion-acoustic solitons, respectively. We observe that the amplitude decreases while the width increases with an increase in κ for both O^+ and H^+ ion-acoustic solitons. In addition, the amplitude and width of the H^+ ion-acoustic soliton is larger than the O^+ ion-acoustic soliton.

Figure 9 depicts the soliton potential variation with v_0 for (a) O^+ and (b) H^+ ion-acoustic solitons corresponding to the normalized parameters of Figure 8. For both O^+ and H^+ ion-acoustic modes, the amplitude increases while the width decreases with increasing v_0 .

Tables 2 and 3 summarize the effective Debye length, λ_{dse} , unnormalized soliton velocity (V), electric field (E), the soliton width (W), the electrostatic potential (ϕ), peak frequency (f_{peak}), corresponding to the maximum power in the spectrum and the time duration ($\tau = W/V$) of slow O^+ and H^+ ion-acoustic solitons at different altitudes for $v_0 = 4.92$ corresponding to $V_0 = 200 \text{ km s}^{-1}$ for both the DD and NM sectors. Here, width is considered as the

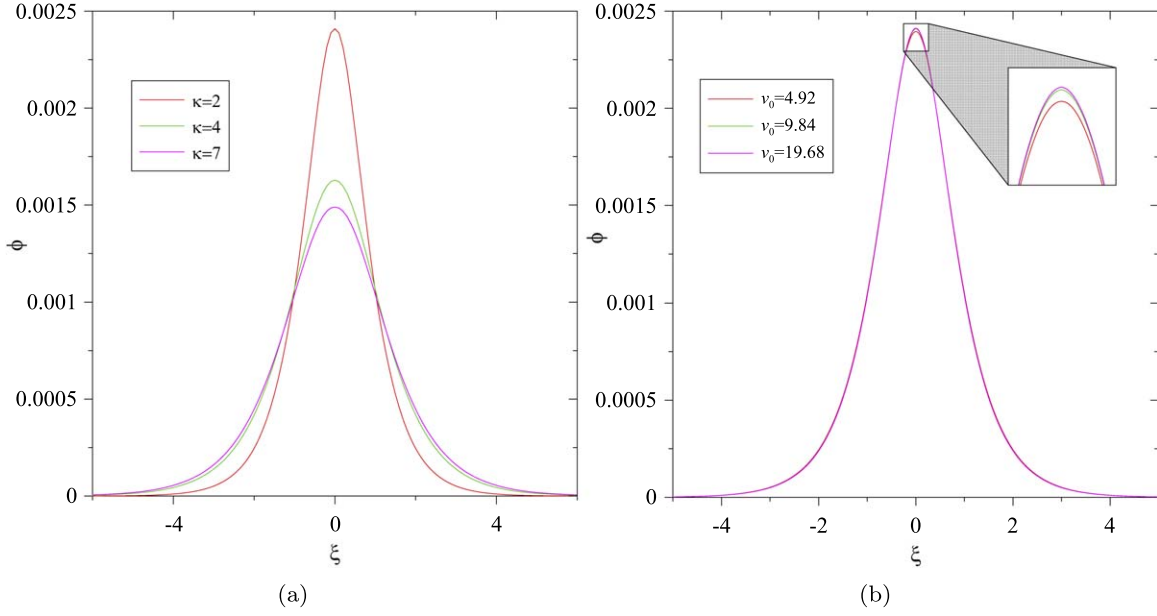


Figure 7. Variation of potential profile with (a) κ and (b) v_0 is shown for H^+ ion-acoustic mode for DD sector at an altitude of 2000 km. The normalized parameters considered are $n_{vh0} = 0.27$, $n_{vo0} = 0.01$, $n_{sp0} = 0.72$, $\sigma_{vh} = \sigma_{vo} = 0.005$, $\sigma_{sp} = 0.5$, $\sigma_{be} = 0.025$, and $M = 0.2$.

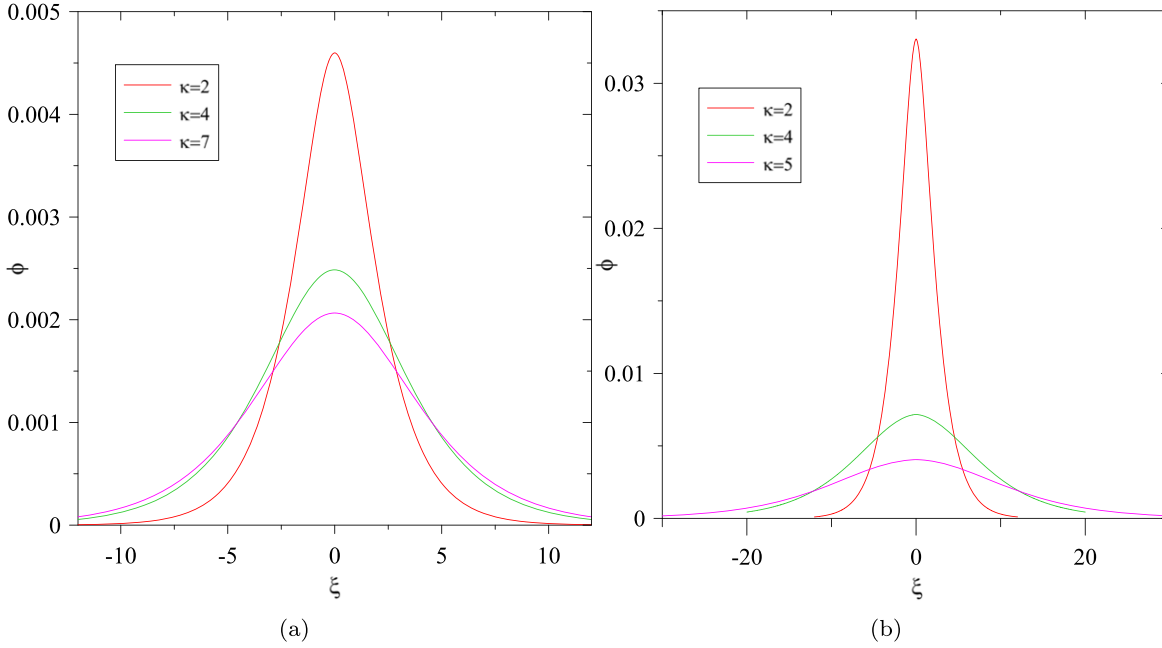


Figure 8. Variation of potential profile with κ for (a) O^+ and (b) H^+ ion-acoustic solitons for the DD sector at an altitude (10^3 - 10^4). The normalized parameters considered are taken from Afify et al. (2021), viz., $n_{vh0} = 0.53$, $n_{vo0} = 0.31$, $n_{sp0} = 0.16$, $\sigma_{vh} = \sigma_{vo} = 0.25$, $\sigma_{sp} = 1$, and $\sigma_{be} = 1$. Here, (a) $M = 0.242$ and (b) $M = 1.13$.

full width at half maximum. For the parameters corresponding to Table 1, with $T_{vh} = T_{vo} = 1000$ K, $T_{be} = 5000$ K, $T_{sp} = 10^5$ K, and $T_{se} = 2 \times 10^5$ K, we have the ion-acoustic speed $C_a = 40.63$ km s^{-1} .

From Table 2, we observe that in the DD sector at an altitude of 200 km, only O^+ ion-acoustic mode exists. While at an altitude of 2000 km, only H^+ ion-acoustic solitons exists. The velocity of the O^+ ion-acoustic solitons increases with a decrease in the altitude, while the velocity of the H^+ ion-acoustic solitons decreases with altitude. The electric field amplitude of the H^+ ion-acoustic solitons decreases with decrease in the altitude. Both O^+ and H^+ ion-acoustic solitons

have positive polarity. The velocity, electric field amplitude, width, potential, peak frequency, and the time duration of O^+ ion-acoustic solitons lie in the range of $\sim(1.58$ – $2.12)$ km s^{-1} , $\sim(4.12$ – $27.67)$ mV m^{-1} , $\sim(1.7$ – $3.74)$ m, $\sim(7.97$ – $43.93)$ mV, $\sim(29.93$ – $54.08)$ Hz, and $\sim(0.94$ – $1.79)$ ms, respectively. The H^+ ion-acoustic solitons have V , E , W , ϕ , f_{peak} , and τ in the range of $\sim(5.37$ – $8.33)$ km s^{-1} , $\sim(0.24$ – $12.25)$ mV m^{-1} , $\sim(1.92$ – $25.49)$ m, $\sim(0.54$ – $56)$ mV, $\sim(87.22$ – $743)$ Hz, and $\sim(0.35$ – $3.32)$ ms, respectively.

From Table 3, we observe that the effective Debye length, λ_{dse} decreases with a decrease in the altitude. The velocity of the O^+ ion-acoustic solitons increases while that of the H^+ ion-acoustic

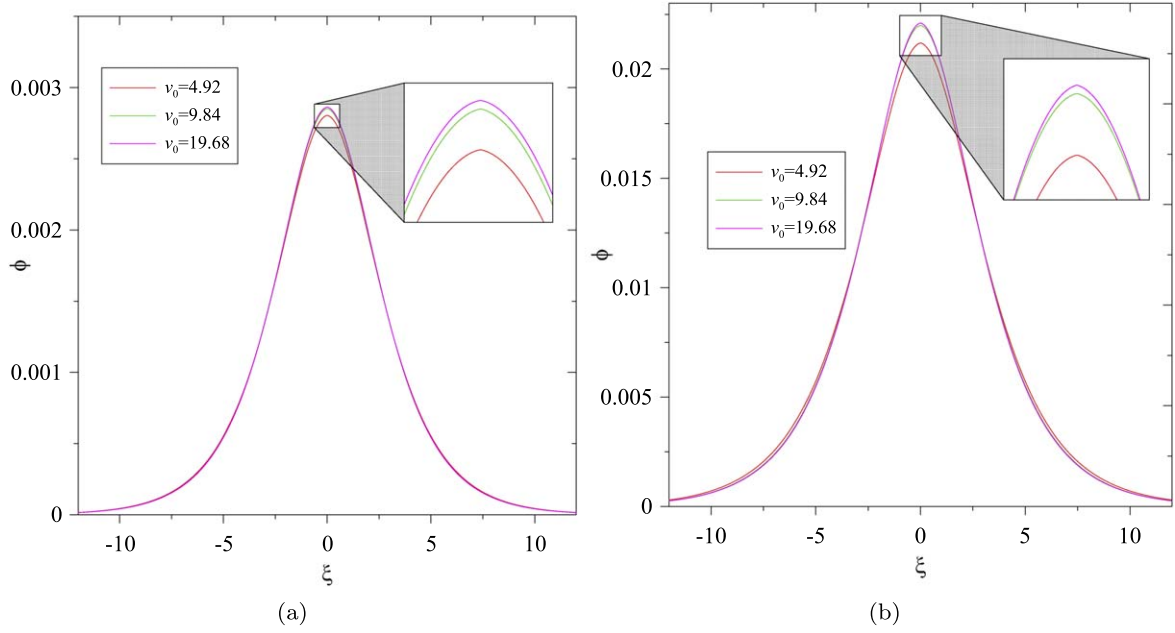


Figure 9. Potential profile varying with for (a) O^+ ($M = 0.24$) and (b) H^+ ($M = 1.11$) ion-acoustic solitons corresponding to the normalized parameters of Figure 8.

Table 2
ESWs' Properties at Different Altitudes of Venus's Ionosphere Permeated by the Solar Wind for the DD Sector

Altitude (km)	Mode	λ_{dsc} (m)	V ($km\ s^{-1}$)	E ($mV\ m^{-1}$)	W (m)	ϕ (mV)	f_{peak} (Hz)	τ (ms)
2000	O^+	4.14
	H^+		(7.68–8.33)	(0.24–12.25)	(25.49–5.71)	(4.59–56)	(144.21–743.02)	(3.32–0.68)
1000	O^+	3.08	(1.58–1.61)	(4.16–7.34)	(2.41–1.85)	(7.97–11.07)	(29.93–40.57)	(1.61–1.58)
	H^+		(6.93–7.07)	(6.22–10.85)	(3.33–2.53)	(16.19–22.41)	(130.92–133.60)	(0.4–0.36)
800	O^+	3.11	(1.58–1.61)	(4.26–7.49)	(2.36–1.80)	(8.02–11.11)	(29.93–40.57)	(1.46–1.14)
	H^+		(6.93–7.07)	(6.12–10.77)	(3.42–2.61)	(18.88–22.27)	(87.22–133.59)	(0.48–0.38)
600	O^+	2.66	(1.81–1.85)	(11.34–21.57)	(2.39–1.70)	(21.25–30.55)	(39.53–54)	(1.3–0.94)
	H^+		(6.04–6.13)	(2.20–3.89)	(2.82–2.13)	(4.92–6.85)	(88.12–134.04)	(0.46–0.35)
400	O^+	2.18	(1.98–2.02)	(13.77–27.67)	(2.66–2.01)	(28.67–43.9)	(35.24–54.08)	(1.32–1.01)
	H^+		(5.37–5.41)	(0.24–0.61)	(2.84–1.92)	(0.54–0.95)	(95.5–144.54)	(0.53–0.35)
200	O^+	2.15	(2.08–2.12)	(8.44–19.33)	(3.74–2.75)	(24.29–40.98)	(37.5–38.28)	(1.76–1.29)
	H^+	

Note. The total number density of the ions for DD sector is obtained from Table 1, i.e., $N_0 = N_{vh0} + N_{vo0} + N_{sp0}$. The temperature of the solar wind electrons $T_{se} = 2 \times 10^5$ K. Here, V is the velocity of the soliton, E is the electric field amplitude, W is the width of the solitons (taken as full width at half maximum), ϕ is the electrostatic potential, f_{peak} is the peak power in the FFT power spectrum of the electric field, and τ is the time duration.

solitons decreases with a decrease in the altitude. The potential of the O^+ ion-acoustic solitons increases with a decrease in the altitude and the potential of the H^+ ion-acoustic solitons decreases with decrease in altitude. The O^+ ion-acoustic solitons have V , E , W , ϕ , f_{peak} , and τ in the range of $\sim(1.48\text{--}2.08)$ $km\ s^{-1}$, $\sim(0.28\text{--}23.02)$ $mV\ m^{-1}$, $\sim(2.44\text{--}32.37)$ m, $\sim(2.67\text{--}43.07)$ mV, $\sim(26.85\text{--}108.14)$ Hz, and $\sim(1.18\text{--}22)$ ms, respectively. Meanwhile, the H^+ ion-acoustic solitons have V , E , W , ϕ , f_{peak} , and τ in the range of $\sim(5.1\text{--}7.39)$ $km\ s^{-1}$, $\sim(0.03\text{--}4.28)$ $mV\ m^{-1}$, $\sim(1.76\text{--}53.21)$ m, $\sim(0.067\text{--}30.5)$ mV, $\sim(65.01\text{--}401.79)$ Hz, and $\sim(0.34\text{--}7.76)$ ms, respectively.

We would like to point out that although VEX did not carry any plasma wave instruments, it provided important information about the plasma composition of ions and electrons in the induced Venusian magnetosphere (Barabash et al. 2007). We

have used this information in our model (Lundin et al. 2011). Our model clearly shows that both slow O^+ and H^+ ion-acoustic solitons can exist in the Venusian ionosphere at various altitudes. In this paper, we have considered the plasma rest frame to be Venus centric. In this frame, the solar wind is flowing with velocity $v_{sw} \approx 400$ $km\ s^{-1}$ just outside the induced Venus magnetosphere. As the solar wind penetrates the induced Venusian magnetosphere/ionosphere, it gets slowed down and deflected. In the satellite frame, all of the frequencies are Doppler shifted and are given by $f_{sc} = f_{pl} + \frac{k \cdot v_{sw}}{2\pi} + \frac{k \cdot v_{sat}}{2\pi}$ (Mozer et al. 2020). Here, f_{sc} and f_{pl} are the frequencies of the ion-acoustic solitary wave in the spacecraft frame and plasma frame, respectively. v_{sat} is the spacecraft velocity, which is less than v_{sw} , and can therefore be neglected. The Doppler shift will be maximum when the wave

Table 3
Electrostatic Solitary Waves Properties at Different Altitudes of the Solar Wind-Venus Ionosphere Interaction Region for the NM Sector

Altitude (km)	Mode	λ_{dsc} (m)	V (km s ⁻¹)	E (mV m ⁻¹)	W (m)	ϕ (mV)	f_{peak} (Hz)	τ (ms)
2000	O ⁺	9.30	(1.48–1.52)	(0.28–1.21)	(32.37–32)	(2.67–6.45)	(61.94–108.14)	(21.9–21)
	H ⁺		(6.85–7.39)	(0.03–4.28)	(53.21–26.23)	(1.28–30.5)	(71.45–401.79)	(7.76–3.55)
1000	O ⁺	3.56	(1.78–1.81)	(9.38–13.11)	(2.99–2.49)	(21.99–26.43)	(29.21–39.45)	(1.65–1.40)
	H ⁺		(6.16–6.26)	(1.78–3.32)	(4.13–3.06)	(5.86–8.43)	(67.14–102.33)	(0.67–0.49)
800	O ⁺	3.43	(1.89–1.93)	(10.9–19.5)	(3.29–2.4)	(28.22–39.13)	(32.14–32.88)	(1.71–1.27)
	H ⁺		(5.73–5.81)	(0.65–1.46)	(4.25–2.95)	(2.19–3.57)	(65.01–98.86)	(0.74–0.51)
600	O ⁺	2.83	(1.96–2)	(10.9–21.42)	(3.46–2.55)	(28.65–43.07)	(26.85–41.21)	(1.73–1.30)
	H ⁺		(5.46–5.49)	(0.42–0.71)	(2.95–2.38)	(1.02–1.38)	(74.79–112.98)	(0.54–0.44)
400	O ⁺	2.18	(2.04–2.07)	(14.4–23.02)	(2.92–2.39)	(31.98–42.96)	(36.44–36.95)	(1.41–1.17)
	H ⁺		(5.18–5.2)	(0.09–0.17)	(2.26–1.82)	(0.18–0.26)	(92.47–139.32)	(1.09–0.35)
200	O ⁺	2.15	(2.06–2.08)	(13.6–20.8)	(3.01–2.58)	(31.45–41.14)	(37.24–37.67)	(1.45–1.25)
	H ⁺		(5.10–5.12)	(0.034–0.067)	(2.41–1.72)	(0.067–0.1)	(92.26–138.68)	(1.45–1.25)

Note. The total number density of the ions for NM sector is obtained from Table 1, i.e., $N_0 = N_{vh0} + N_{vo0} + N_{sp0}$. The temperature of the solar wind electrons $T_{se} = 2 \times 10^5$ K.

is propagating either parallel or antiparallel to v_{sw} , and it will be zero when it propagates transverse to v_{sw} . Therefore, to get an estimate of the Doppler shift, we have calculated the Doppler shift at an altitude of 1000 km in the DD sector for both the O⁺ and H⁺ modes. At 1000 km, the bulk velocities of the plasma varies in the range of $\sim(100\text{--}200)$ km s⁻¹ (Martinez et al. 2009; Lundin et al. 2011). The Doppler shift is given by Tsurutani et al. (1983): $f_{sc} = f_{pl} (1 + (v_{sw}/v_{ph})\cos\theta)$. Here, θ is the angle between the wave propagation direction and solar wind velocity vector. At an altitude of 1000 km, for $v_0 = 4.92$ (approximately corresponding to a solar wind flow velocity of ~ 200 km s⁻¹), the O⁺ and H⁺ ion-acoustic solitons have plasma rest frame frequencies near the peak of the spectra as 40.57 Hz and 133.60 Hz, respectively. In the spacecraft frame, the frequencies of O⁺ and H⁺ solitons are Doppler shifted to 5.08 kHz and 3.91 kHz, respectively. It should be noted that this estimate is for the maximum Doppler shift corresponding to $\cos\theta = 1$. For other cases, the maximum Doppler shifts would be reduced by a factor of $\cos\theta$. Thus, the Doppler shifted frequencies corresponding to the peaks in the power spectra in the plasma rest frame compare well with the PVO observations of ion-acoustic waves with frequencies 5.4 kHz. The ion-acoustic solitons that are predicted by our model can explain the PVO observation of ion-acoustic waves in the frequency range of 100 Hz, 730 Hz, and 5.4 kHz (Scarf et al. 1979; Strangeway 1991; Yadav 2020) with an electric field amplitude of $10^{-1}\text{--}10^{-2}$ mV m⁻¹. In addition, the model (see the H⁺ ion-mode in Tables 2 and 3) can be relevant in explaining the Solar Orbiter observation of ESWs with a peak-to-peak electric field amplitude of a few mV m⁻¹ with a characteristic timescale of ~ 0.5 ms in the magnetosheath region (Hadid et al. 2021).

4. Comparison with Previous Theoretical Studies of the ESWs Occurring in the Solar-Venus Plasma Environment

Afify et al. (2021) analyzed small amplitude (KdV type) compressive (positive) solitons during solar wind interaction with Venus's atmosphere at high altitudes ($10^3\text{--}10^4$ km) for DD sector. They considered unmagnetized plasma comprising of O⁺ and H⁺ ions and inertialess electrons of Venusian origin,

and solar wind protons and electrons. The phase velocity (Mach number) and the temperature ratio of the Venusian H⁺ and the background electrons was found to significantly affect the amplitude of the solitons. They reported solitons with maximum electric field amplitude ~ 1.2 mV m⁻¹ and time duration of ~ 0.4 ms. The FFT of electric field profile generated a broadband electrostatic noise with a frequency range of $\sim(3.2\text{--}199.5)$ kHz and peak frequency of ~ 40 kHz. In our model, we have considered Maxwellian background electrons, and streaming solar wind protons and suprathermal electrons in line with the observations. Furthermore, we have analyzed the occurrence and characteristics of arbitrary amplitude O⁺ and H⁺ ion-acoustic solitons in both DD and NM sectors for an altitude of $\sim(200\text{--}2000)$ km. We observe that the H⁺ ion-acoustic solitons have electric field amplitudes and timescales similar to those reported by Afify et al. (2021). However, the frequency observed is less than that of Afify et al. (2021) because they had considered higher total number density of the ions $\sim 10^4$ cm⁻³. Both small and arbitrary amplitude ion-acoustic solitons in an unmagnetized plasma consisting of H⁺ and O⁺ ions and Maxwellian electrons in the NM meridian at an altitude of $\sim(200\text{--}1000)$ km were studied by Sayed et al. (2020), who reported compressive (positive) solitons with an electric field amplitude of 44 mV m⁻¹. In addition, the amplitude of the solitons was observed to increase, while the width decreases with an increase in Mach number. However, we observe that the electric field amplitude of the solitons in the NM sector from our model is less than that reported by Sayed et al. (2020) on account of the Venusian background electron temperature, $T_e = 10^4$ K considered by them is twice as large as ours. In addition, Sayed et al. (2020) did not consider the effect of streaming solar wind particles on the Venusian ionosphere. Fayad et al. (2021) studied weakly nonlinear ion-acoustic solitons in the Venus ionosphere assumed to be composed of streaming O⁺ and H⁺ ions and Maxwellian electrons using Zakharov–Kuznetsov equation. They reported compressive solitons with an electric field amplitude $\sim(7.63\text{--}11.52)$ mV m⁻¹ occurring at an altitude of (400–1000) km in DD meridian of the Venusian atmosphere. The amplitude and width of the solitons were found to decrease with an increase in altitude.

Similar characteristics are shown by O^+ ion-acoustic solitons in both DD and NM sector in our model. In addition, the electric field amplitude matches well with that reported by Fayad et al. (2021). Streaming ion velocities were reported to enhance the amplitude and energy of the solitons by Fayad et al. (2021). In our case, the streaming velocity of the solar wind particles only has a significant affect on the soliton characteristics when their number density is above a threshold value ($n_{sp0} > 0.15$). Prasad et al. (2021) studied the occurrence of large amplitude rarefactive solitons at an altitude of (200–1000) km in the NM meridian of the Venusian atmosphere as a consequence of ionospheric escape. They modeled the interaction of the solar wind with Venus's atmosphere using H^+ and O^+ ions, electrons, and solar wind protons and electrons. All of the species were considered as streaming. Our model supports only positive potential solitons. Salem et al. (2022) carried out parametric analysis for the existence domain of positive potential ion-acoustic solitons in the NM sector of the transition zone (the mantle, 1000–2000 km) existing between the ionosphere and the magnetosheath region of Venus. The soliton amplitude was observed to decrease with an increase in the temperature of either the solar wind protons or electrons. The soliton amplitude was observed to only be affected by the solar wind proton flow velocity, u_{sp0} variation, in a particular velocity range, which is referred to as the velocity scale. The number density ratio of the solar wind electron to that of the O^+ ions ($\beta = n_{se0}/n_{O0}$) did not affect the characteristics of the ion-acoustic solitons. Meanwhile, the electric field amplitude of the solitons was observed to increase with the number density ratio of solar wind protons to the O^+ ions ($\delta = n_{sp0}/n_{O0}$). From our model, we observed that the solar wind particles only affect the soliton characteristics when the number density of the solar wind particles is above a threshold density ($n_{sp0} > 0.15$) and when the temperature of the solar wind protons become comparable to the that of the Venusian background electrons.

All of these models analyzed ion-acoustic solitons in either DD or NM meridian of the Venusian ionosphere. In addition, all of these studies considered a single wave mode, viz., ion-acoustic mode. In this paper, we have analyzed the characteristics of both slow O^+ and H^+ ion-acoustic solitons in both NM and DD sectors. Furthermore, in the previous studies, the authors considered the fact that temperature of the solar wind electron and proton equalizes with that of the background Venusian electrons at altitudes less than 2000 km (Afify et al. 2021; Salem et al. 2022). In the absence of observational data for temperature variation with altitude, we have analyzed the characteristics of the solitons considering both higher solar wind electron temperature (Figures 2–7) and when the temperature of the solar wind particle equalizes that of the background Venusian electrons (Figures 8 and 9). We observe that when equal temperature is considered, the amplitude and width of the solitons is higher than when higher solar wind electron temperature is considered. We also emphasize that the number density and relative temperature of the ionospheric and solar wind particles play a vital role in the generation of ESWs during solar wind interaction with the Venus ionosphere. This study is pertinent because satellite observations of the ESWs occurring in the lower Venusian ionosphere (below 1000 km) are not available in the literature to the best of our knowledge and these studies could form the basis for future observations of ESWs in the lower Venusian ionosphere.

5. Conclusions


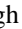
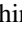
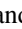
We have studied the characteristics of ESWs in the Venus ionosphere permeated by the solar wind. The main results of this study are summarized below:

1. Venus's ionosphere when impinged by the solar wind supports the existence of positive potential slow O^+ and H^+ ion-acoustic solitons.
2. The characteristics of the solitons are significantly affected by the solar wind particles when their density relative to total ion density is above a threshold value ($n_{sp0} > 0.15$), and the temperature of the solar wind particles and background Venusian electrons becomes comparable.
3. The amplitude of the O^+ ion-acoustic solitons in the DD meridian is less than that of the solitons in NM meridian for a given altitude.
4. The amplitude of the H^+ ion-acoustic solitons in the DD meridian is greater than that of the solitons in NM meridian for a given altitude.
5. For the plasma parameters pertinent to the DD and NM sectors of the Venus ionosphere as provided by Lundin et al. (2011), our model supports the simultaneous existence of slow O^+ and H^+ ion-acoustic solitons. Taken together, the amplitude of potential, width, and velocity of the ion-acoustic solitons varies as $\sim(0.067\text{--}56)$ mV, $\sim(1.70\text{--}53.21)$ m, and $\sim(1.48\text{--}8.33)$ km s⁻¹, respectively. The bipolar electric field amplitude varies as $\sim(0.03\text{--}27.67)$ mV m⁻¹ with time durations $\sim(0.34\text{--}22)$ ms. The FFT of the electric field generates power spectra with peaks varying between $\sim(26.85$ and $743)$ Hz for various soliton velocities.
6. This model can be used to explain the PVO observation of ion-acoustic waves with frequency ~ 100 Hz–5.4 kHz having an electric field amplitude of $10^{-1}\text{--}10^{-2}$ mV m⁻¹. This model is generic, and can therefore be relevant in explaining the observation of ESWs in the magnetosheath region by the Solar Orbiter during gravity assist maneuver of Venus if the observed plasma parameters are taken as an input.

Acknowledgments

R.R. thanks Department of Science and Technology (DST), Government of India, India for the support under INSPIRE-Faculty Fellowship. G.S.L. thanks the Indian National Science Academy (INSA), New Delhi, India for the support under the INSA-Honorary Scientist Scheme. The authors would like to thank Dr. Padma Gurram for her help in FFT.

ORCID iDs

R. Rubia  <https://orcid.org/0000-0002-8584-3319>
 S. V. Singh  <https://orcid.org/0000-0003-2758-7713>
 G. S. Lakhina  <https://orcid.org/0000-0002-8956-486X>
 S. Devanandhan  <https://orcid.org/0000-0001-9061-7140>

References

- Afify, M., Elkamash, I., Shihab, M., & Moslem, W. 2021, *AdSpR*, **67**, 4110
 Barabash, S., Fedorova, A., Sauvaud, J. J., et al. 2007, *Natur*, **450**, 650
 Brace, L. H., Theis, R. F., & Hoegy, W. R. 1982, *P&SS*, **30**, 29
 Elphic, R. C., Russell, C. T., & Slavin, J. A. 1980, *JGR*, **85**, 7679

- Fayad, A. A., Moslem, W. M., & El-Labany, S. K. 2021, *PhyS*, **96**, 045602
- Futaana, Y., Wieser, G. S., Barabash, S., & Luhmann, J. G. 2017, *SSRv*, **212**, 1453
- Gurnett, D. A., Kurth, W. S., Roux, A., et al. 1991, *Sci*, **253**, 1522
- Hadid, L. Z., Edberg, N. J. T., Chust, T., et al. 2021, *A&A*, **656**, A18
- Hashimoto, K., Hashitani, M., Kasahara, Y., et al. 2010, *GeoRL*, **37**, L19204
- Intriligator, D. S., & Scarf, F. L. 1984, *JGR*, **89**, 47
- Knudsen, W. C. 1992, *GMS*, **66**, 237
- Kurth, W. S., Gurnett, D. A., Persoon, A. M., et al. 2001, *P&SS*, **49**, 343
- Lakhina, G. S., & Singh, S. V. 2015, *SoPh*, **290**, 3033
- Lakhina, G. S., Singh, S. V., Kakad, A. P., et al. 2009, *JGRA*, **114**, A09212
- Lakhina, G. S., Singh, S. V., & Kakad, A. P. 2014, *PhPI*, **21**, 062311
- Lakhina, G. S., Singh, S. V., Kakad, A. P., Verheest, F., & Bharuthram, R. 2008, *NPGeo*, **15**, 903
- Lakhina, G. S., Singh, S. V., & Rubia, R. 2020, *PhyS*, **95**, 105601
- Lakhina, G. S., Singh, S. V., & Rubia, R. 2021a, *AdSpR*, **68**, 1864
- Lakhina, G. S., Singh, S. V., Rubia, R., & Devanandhan, S. 2021b, *Plasma*, **4**, 681
- Lakhina, G. S., Singh, S. V., Rubia, R., & Sreeraj, T. 2018, *PhPI*, **25**, 080501
- Lakhina, G. S., Tsurutani, B. T., Kojima, H., & Matsumoto, H. 2000, *JGR*, **105**, 27791
- Leubner, M. P. 1982, *JGR*, **87**, 6335
- Liu, Z., & Du, J. 2009, *PhPI*, **16**, 123707
- Luhmann, J. G. 1986, *SSRv*, **44**, 241
- Luhmann, J. G., & Kozyra, J. U. 1991, *JGR*, **96**, 5457
- Lundin, R., Barabash, S., Futaana, Y., et al. 2011, *Icar*, **215**, 751
- Maksimovic, M., Pierrard, V., & Lemaire, J. F. 1997a, *A&A*, **324**, 725
- Maksimovic, M., Pierrard, V., & Riley, P. 1997b, *GeoRL*, **24**, 1151
- Malaspina, D. M., Goodrich, K., Livi, R., et al. 2020, *GeoRL*, **29**, 47
- Mangeney, A., Salem, C., Lacombe, C., et al. 1999, *AnGeo*, **17**, 307
- Martinez, C., Boesswetter, A., Franz, M., et al. 2009, *JGRA*, **114**, E00B30
- Matsumoto, H., Kojiima, H., Miyatake, T., et al. 1994, *GeoRL*, **21**, 2915
- Moslem, W. M., Rezk, S., Abdelsalam, U. M., & El-Labany, S. 2018, *AdSpR*, **61**, 2190
- Mozer, F. S., Bonnell, J. W., Bowen, T. A., Schumm, G., & Vasko, I. Y. 2020, *ApJ*, **901**, 107
- Phillips, J. L., & Russell, C. T. 1987, *JGR*, **92**, 2253
- Pickett, J. S., Chen, L.-J., Kahler, S. W., et al. 2005, *NPGeo*, **12**, 181
- Pierrard, V., & Lemaire, J. 1996, *JGR*, **101**, 7923
- Prasad, P. K., Abdikian, A., & Saha, A. 2021, *AdSpR*, **68**, 4155
- Reddy, R. V., & Lakhina, G. S. 1991, *P&SS*, **39**, 1343
- Rubia, R., Singh, S. V., & Lakhina, G. S. 2016, *PhPI*, **23**, 062902
- Rubia, R., Singh, S. V., & Lakhina, G. S. 2017, *JGRA*, **122**, 9134
- Rubia, R., Singh, S. V., & Lakhina, G. S. 2018, *PhPI*, **25**, 032302
- Russell, C., Luhmann, J., & Strangeway, R. 2006, *P&SS*, **54**, 1482
- Russell, C. T., Luhmann, J. G., Elphic, R. C., Scarf, F. L., & Brace, L. H. 1982, *GeoRL*, **9**, 45
- Salem, S., Fayad, A. A., El-Shafeay, N. A., et al. 2022, *MNRAS*, **517**, 2876
- Salem, S., Moslem, W., Lazar, M., et al. 2019, *AdSpR*, **65**, 129
- Sayed, F., Turkey, A., Koramy, R., & Moslem, W. 2020, *AdSpR*, **66**, 1276
- Scarf, F. L., Neumann, S., Brace, L. H., et al. 1985, *AdSpR*, **5**, 185
- Scarf, F. L., Taylor, W. L., & Green, I. M. 1979, *Sci*, **203**, 748
- Singh, S. V., Rubia, R., Devanandhan, S., & Lakhina, G. S. 2020, *PhyS*, **95**, 075602
- Strangeway, R. J. 1991, *SSRv*, **55**, 275
- Summers, D., & Thorne, R. M. 1991, *PhFIB*, **3**, 1835
- Tsurutani, B. T., Smith, E. J., & Jones, D. E. 1983, *JGR*, **88**, 5645
- Vasyliunas, V. M. 1968, *JGR*, **73**, 2839
- Williams, J. D., Chen, L. J., Kurth, W. S., Gurnett, D. A., & Dougherty, M. K. 2006, *GeoRL*, **33**, L06103
- Yadav, V. K. 2020, *IETE Tech. Rev.*, **38**, 622
- Zhang, T. L., Delva, M., Baumjohann, W., et al. 2007, *Natur*, **450**, 654